Pressure induced Invar effect in $Fe_{55}Ni_{45}$: An experimental study with nuclear resonant scattering

P. Guzman,* S. H. Lohaus, C. M. Bernal-Choban, and B. Fultz
California Institute of Technology, Pasadena, California 91125, USA

J. Y. Zhao, G. Shen, M. Y. Hu, and E. E. Alp
Advanced Photon Source, Argonne National Laboratory, Argonne, Illinois 60439, USA

B. Lavina
Center for Advanced Radiation Sources, The University of Chicago, Chicago, IL 60637, USA and Advanced Photon Source, Argonne National Laboratory, Argonne, Illinois 60439, USA
(Dated: November 22, 2024)

Pressure-dependent synchrotron X-ray diffraction (XRD), nuclear resonant inelastic X-ray scattering (NRIXS), and nuclear forward scattering (NFS) measurements were made on $^{57}Fe_{55}Ni_{45}$. XRD measurements were at 298 K and 392 K at pressures up to 20 GPa, confirming a pressure-induced Invar effect between 7 GPa and 13 GPa. A decrease of the ^{57}Fe magnetic moment was found in NFS measurements under pressure, showing an increase in magnetic entropy. The ^{57}Fe phonon density of states (DOS) was obtained from NRIXS measurements. The low thermal expansion in the high-pressure Invar region originates from a competition between the thermal expansion from spins and phonons as calculated from Maxwell relations. The longitudinal phonon modes changed their pressure dependence near the Curie transition, which is evidence for a spin-phonon interaction.

I. INTRODUCTION

A. Invar effect

The fcc alloy $Fe_{64}Ni_{36}$ exhibits the classic Invar effect, where its thermal expansion is nearly zero at ambient conditions. In 1920, Charles-Édouard Guillaume was awarded the Nobel Prize "in recognition of the service he has rendered to precision measurements in Physics by his discovery of anomalies in nickel steel alloys" [1–3]. Invar alloys of $Fe_{64}Ni_{36}$ have long been used for precision instruments and devices that maintain their dimensional stability over a range of temperatures [4].

Guillaume found that the Invar effect was lost for non-magnetic states of the material, and understood that there was a role for magnetism in thermal expansion to counteract the expected positive thermal expansion of the alloy. Recently, the phonon and magnetic contributions to thermal expansion in Invar were isolated, and shown to cancel [5]. Furthermore, interactions between spins and phonons were shown to extend the range of pressures for near-zero thermal expansion in $Fe_{65}Ni_{35}$ from 0 to 3 GPa (the Curie pressure was reported to be 4.6 GPa). Invar behavior has been reported in other systems such as Fe-Pt, Fe-Co, Ni-Mn and hcp Gd [6–14]. Many amorphous materials containing iron show Invar anomalies at ambient pressure. References [4, 15–19] provide a thorough review of experimental and theoretical work on the Invar problem.

Both lattice dynamics and magnetism are changed with pressure. Under pressure, it was reported that Invar behavior develops in $Fe_{55}Ni_{45}$, $Fe_{20}Ni_{80}$, and Pd_3Fe [20–22], and effects of pressure on materials with the ambient Invar effect have been investigated in numerous previous studies [23–40].

Here we present a study of the pressure-induced Invar effect in $Fe_{55}Ni_{45}$, first reported in 2001 [20]. By comparing x-ray lattice parameters from samples in a diamond-anvil cell at two temperatures, we found an anomalous thermal expansion occurring at pressures between 7 and 13 GPa. Nuclear forward scattering (NFS) showed that a Curie transition in $Fe_{55}Ni_{45}$ occurs at 13 GPa in pressure, so there should be an increase in spin disorder and magnetic entropy just below this pressure. From [41] it is known that the Curie temperature of $Fe_{55}Ni_{45}$ is 700 K. Nuclear resonant inelastic x-ray scattering (NRIXS) was used to measure the partial phonon density of states (DOS) of ^{57}Fe atoms. The NRIXS spectra showed an arrest in the increase of longitudinal phonon modes between 7 and 13 GPa, but the average phonon entropy decreased as the frequencies of other phonons increased with pressure. The decrease of phonon entropy counteracted precisely the pressure-dependence of the magnetic entropy, which increased from spin disorder as the Curie transition was approached. A Maxwell relation shows that magnetism and phonons therefore have canceling contributions to thermal expansion near 10 GPa. The behavior is similar to what was observed below the Curie pressure in $Fe_{65}Ni_{35}$ [5] at pressures up to 3 GPa. The arrest of the longitudinal phonon frequencies is interpreted as evidence of spin-phonon interactions.

Finally, the alloy $Fe_{55}Ni_{45}$ is known as "Elinvar" because it has no change of its elastic constants at temperatures near ambient. We show in the Supplemental Material [42] that the Elinvar behavior occurs at low pressures, but the NRIXS and NFS measurements were not

* pgguzman@caltech.edu

sufficiently precise to pinpoint its thermodynamic origins.

B. Thermophysics of thermal expansion

The fractional change in volume V with temperature T is the volume coefficient of thermal expansion, β:

$$\beta = \frac{1}{V}\left(\frac{\partial V}{\partial T}\right)_{\mathrm{P}} \tag{1}$$

The phonon and spin contributions to the thermal expansion can be found experimentally by use of a thermodynamic Maxwell relation [5]

$$\left(\frac{\partial V}{\partial T}\right)_{\mathrm{P}} = -\left(\frac{\partial S}{\partial P}\right)_{\mathrm{T}}, \tag{2}$$

so β can expressed as

$$\beta = -\frac{1}{V}\left(\frac{\partial S}{\partial P}\right)_{\mathrm{T}} \tag{3}$$

The entropy is dominated by vibrational and magnetic degrees of freedom. (the pressure dependence of the electronic contribution was found to be negligible [5]):

$$\beta = -\frac{1}{V}\left[\left(\frac{\partial S_{\mathrm{ph}}}{\partial P}\right)_{\mathrm{T}} + \left(\frac{\partial S_{\mathrm{mag}}}{\partial P}\right)_{\mathrm{T}}\right] \tag{4}$$

The contribution of phonons is measured through nuclear resonant inelastic x-ray scattering (NRIXS), while the contribution of spins is measured through nuclear forward scattering (NFS).

II. EXPERIMENTAL

A. Sample preparation

The $Fe_{55}Ni_{45}$ alloy was prepared by arc melting high-purity Ni (99.99%) and enriched 95.73% ^{57}Fe (from Isoflex) under an argon atmosphere. (The intensities of NRIXS and NFS spectra are increased by enriching with the ^{57}Fe isotope, which has a natural abundance of only 2.2%.) Foil samples of 15-20 μm thickness were prepared by cold-rolling the arc-melted ingots, and subsequently annealing at 600°C for 12 h in vacuum-sealed quartz ampoules. X-ray diffractometry (XRD) was used to confirm the fcc crystal structure of $Fe_{55}Ni_{45}$.

Pieces of approximately 50×50 μm square were cut from the samples and loaded into diamond anvil cells (DACs) for in-situ experiments with NRIXS, NFS, and XRD. The DACs, symmetric-type and panoramic cells, were loaded with pressure transmitting helium using the COMPRES-GSECARS gas loading system [43] as the pressure medium to better ensure hydrostatic pressures at the sample. Beryllium gaskets were used for NRIXS and NFS to minimize the absorption of x-ray and γ-ray signals emitted from the samples. Holes were drilled in the Be gaskets by laser micromachining system to create a sample chamber, using facilities at sector 16 (High-Pressure Collaborative Access Team) of the Advanced Photon Source (APS) [44]. To determine the pressure inside the sample chamber, two ruby spheres were placed near the sample, and a Raman spectrometer was used to measure and analyze their optical fluorescence spectra. The pressure reported is the average of the two ruby spheres.

B. Synchrotron measurements

The small size of the x-ray beam at the APS allows for measurements on small samples under controlled pressures in DACs. XRD patterns at multiple pressures were measured at beamline 16-BMD (HPCAT) of the APS. The symmetric-type DACs with samples loaded were placed directly in the beam path for measurements at room temperature (RT≃295 K) and in a heating block for measurements at 392 K. Lattice parameters were determined from the (111) diffraction peaks, which gave the strongest intensities and most consistent peak shapes. Peak centers were determined by fitting these peaks to Gaussian functions. $Fe_{55}Ni_{45}$ has a cubic structure, so the unit cell volume was obtained from the lattice parameter cubed. Peak centers were used to quantify how the unit cell volume changed with pressure, and how the material expanded with an increase in temperature of 97 K.

The partial phonon densities of states (DOS) of ^{57}Fe were obtained by NRIXS measurements at beamline 3 ID-B of the APS at Argonne National Laboratory. The NRIXS spectra were collected with three avalanche photodiode detectors positioned at the side openings of the panoramic DACs, perpendicular to the incident X-ray beam. The NRIXS spectra were acquired by scanning the energy of the incident beam across the nuclear resonance of ^{57}Fe at 14.41 keV [45]. The energy resolution of the inelastic spectra was approximately 1.1 meV with the high-resolution monochromator. The PHOENIX software package [46] was used to remove the resonant elastic peak at 14.41 keV, subtract the background, and correct for multiphonon scattering to get the DOS of ^{57}Fe.

The pressure dependence of the ^{57}Fe hyperfine magnetic field (HMF) of $^{57}Fe_{55}Ni_{45}$ was obtained by NFS measurements, also performed at beamline 3 ID-B of the APS. NFS measures the time beats that arise from interferences between γ-ray emissions of different ^{57}Fe nuclei during their transitions from excited to ground states [45]. These time beats are superimposed on an exponential decay from the lifetime of the excited state. The CONUSS software package [46] was used to analyze the beat patterns by fitting with two asymmetrized Gaussians. The mean HMF at each pressure was determined as the average of this model HMF distribution.

III. RESULTS

A. X-ray lattice parameter, NRIXS, and NFS

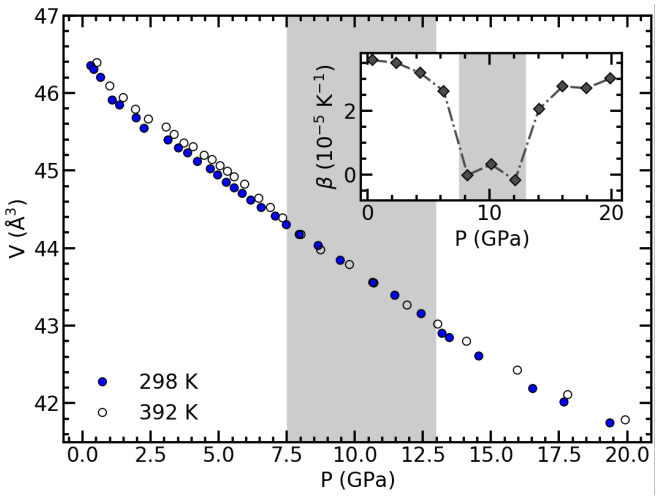

FIG. 1. Pressure dependence of the unit cell volume of Fe-45%Ni at RT (filled circles) and 392 K (open circles). Inset: Pressure dependence of the coefficient of thermal expansion (CTE) measured by XRD. A pressure induced Invar effect is observed between 7 and 13 GPa (shaded area).

Figure 1 shows the unit cell volume from x-ray lattice parameter data as a function of pressure and temperature. At pressures below 3 GPa, the curvatures of the unit cell volume as a function of pressure, which is inversely related to the bulk modulus, are similar between RT and 392 K. An analysis on the curvature of the unit cell volume as a function of pressure is discussed in the Supplemental Material [42]. At pressures between 7 and 13 GPa, the unit cell volume shows no detectable thermal expansion between RT and 392 K. At pressures below 7 GPa and above 13 GPa, however, the volume increases with temperature, becoming a more typical $\beta = 3\text{x}10^{-5}K^{-1}$. Figure 1 inset shows the coefficient of thermal expansion calculated with Eq. (1) between RT and 392 K. A spline interpolation was used to determine the difference between the unit cell volumes as a function of pressure at RT and 392 K.

The NRIXS and NFS spectra were collected consecutively under the same experimental conditions from the same sample. Figure 2 shows phonon DOS curves measured by NRIXS at pressures up to 24 GPa. These spectra show a general increase in energy with increasing pressure. The vertical dashed line is a reference that shows how there is little change in the center of the peak from longitudinal phonon modes between 7.2 and 12.8 GPa. Pairs of DOS curves, shown in the Supplemental Material [42], show this same trend.

Figure 3 shows the NFS spectra at different pressures. Clear magnetic beat patterns are seen at pressures below 14.9 GPa. The beats spread apart in time as the HMF is reduced by increased pressure. Values of the HMF were obtained from the CONUSS fits shown as the solid lines in Fig. 3. This trend is caused by a reduction in HMF with pressure, which is shown in Fig. 4.

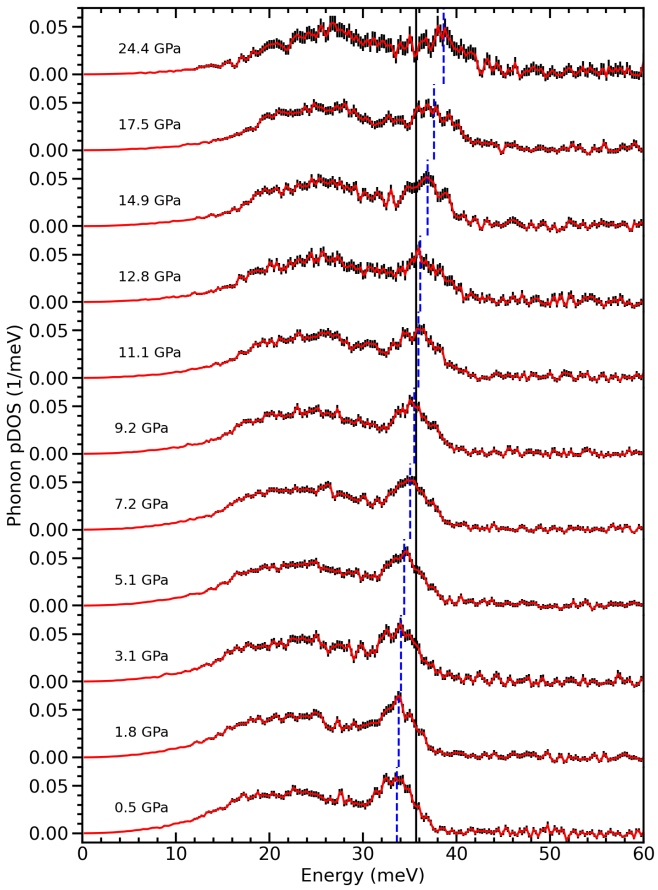

FIG. 2. Pressure dependence of the ^{57}Fe DOS of Fe-45%Ni obtained by Phoenix software from NRIXS measurements at RT. The black vertical line is fixed at the average of the peak position of the longitudinal modes from the 9.2 and 11.1 GPa DOS curves. The maximum of the longitudinal mode for each DOS curve is shown by the blue vertical dashed line. Error bars are shown in black.

B. Phonon entropy

The NRIXS method is an incoherent scattering that provides the phonon spectrum of the solid projected onto the resonant ^{57}Fe nuclei. Contributions from the other atoms in an alloy are not directly measured in an NRIXS spectrum, and this might be a concern in obtaining a thermodynamic vibrational entropy from an alloy if the other elements differed in their vibrational spectra. Fortunately, a prior study compared the inelastic spectra from NRIXS to inelastic neutron scattering spectra of Fe-Ni alloys showed that the phonon partial DOS of Ni and Fe have the same shape [47]. For $Fe_{55}Ni_{45}$, the total phonon DOS is therefore the same as that obtained by

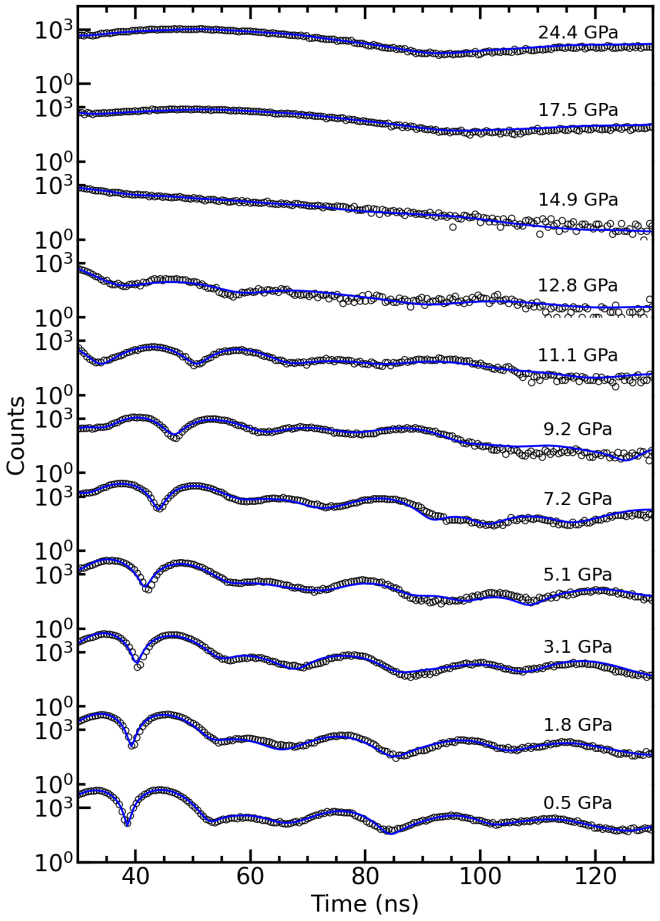

FIG. 3. Pressure dependence of the time signal of $Fe_{55}Ni_{45}$ measured with NFS at RT, with CONUSS fits (blue solid curves) to the beat patterns.

NRIXS. This was also confirmed in recent report [5] by comparing spectra from inelastic neutron scattering and NRIXS for $Fe_{64}Ni_{36}$. The phonon entropy, S_{ph}, is then determined from the phonon DOS, g(ϵ), as [48]

$$S_{\rm ph} = 3k_{\rm B}\int_0^\infty g(\epsilon)\big[(1+n_{\epsilon,T})\ln(1+n_{\epsilon,T}) - n_{\epsilon,T}\ln n_{\epsilon,T}\big]\,d\epsilon \qquad (5)$$

where ϵ is the phonon energy, and $n_{\epsilon,T} = 1/(\exp(\epsilon/k_{\rm B}T)$-1) is the Planck distribution for phonon occupancy. Figure 5 shows the pressure dependence of the $S_{\rm ph}(P)$ obtained from Eq. (5) with the phonon DOS data of Fig. 2. The curve of $S_{\rm ph}(P)$ vs. P is nearly linear. Subtle deviations from linearity are observed in the range of 7 to 13 GPa, corresponding to the range of the pressure-induced Invar effect.

C. Magnetic entropy

Figure 4 shows the average ^{57}Fe HMF as a function of pressure, obtained from CONUSS fits to the NFS spectra. The HMF is proportional to the magnetic moment of Fe atoms [49], so Fig. 4 shows that pressure causes the magnetization to decrease, and magnetization is lost above the Curie pressure of 13 GPa. The magnetization $M(P)$ and the magnetic entropy $S_{\rm mag}$ were determined from the data of Fig. 4 as in [50], which used a mean-field model with spin disordering that corresponds to the

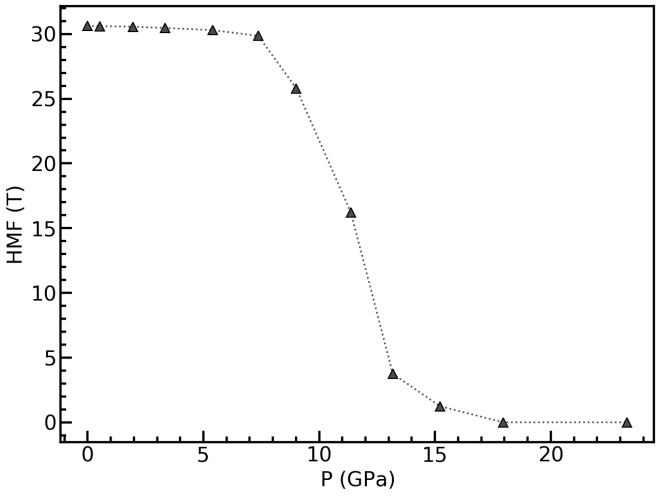

FIG. 4. Pressure dependence of the HMF in $Fe_{55}Ni_{45}$ quantified from NFS with CONUSS measured at RT.

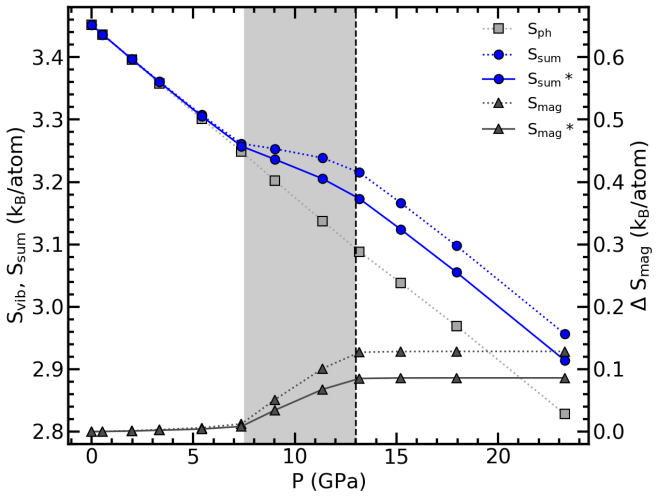

FIG. 5. Pressure dependence of the vibrational entropy (squares), magnetic entropy (triangles), and their sum (circles) obtained from NRIXS and NFS measured at RT. The shading marks the pressure induced Invar region. The dashed vertical line marks the Curie pressure. $S_{\rm mag}$ and $S_{\rm sum}$ was determined with $S_{\rm mag}^{\Delta T}$ from [41]. The $S_{\rm mag}{}^*$ and $S_{\rm sum}{}^*$ were determined with $S_{\rm mag}^{\Delta T}$ from [5].

decreasing magnetization $M(P)$:

$$\Delta S_{\rm mag}(P) = -\frac{S_{\rm mag}^{\Delta \rm T}}{2\ln 2}\left[(1+\mathrm{M(P)})\ln\left(\frac{1+\mathrm{M(P)}}{2}\right)\right. \\ \left.+(1-\mathrm{M(P)})\ln\left(\frac{1-\mathrm{M(P)}}{2}\right)\right] \quad (6)$$

This model does not include magnetic short-range order, and is therefore valid only below the Curie temperature ($T_{\rm C}$). The change in magnetic entropy from RT to $T_{\rm C}$ ($S_{\rm mag}^{\Delta \rm T}$) is obtained from the magnetic heat capacity, and is used to calibrate the change in entropy below the Curie pressure in Eq. (6). It was found in previous experimental studies on fcc Fe-Ni alloys that, for concentrations greater than 44.7% Ni, a significant and inseparable contribution to the specific heat is caused by heat evolution from chemical short-range ordering [41]. It was suggested that it is impractical to extract the magnetic heat capacity from the specific heat for Fe-Ni alloys with Ni concentrations of 44.7% or greater due to chemical short-range ordering. To obtain $S_{\rm mag}^{\Delta T}$ for $Fe_{55}Ni_{45}$, we averaged the specific heat data for $Fe_{61.1}Ni_{38.9}$ and $Fe_{66.2}Ni_{33.8}$ from [41] because their heat capacities were not influenced by atomic ordering. $S_{\rm mag}^{\Delta T} = 0.128\ k_{\rm B}$/atom was obtained for $S_{\rm mag}^{\Delta T}$ by averaging the specific heats of 38.9% Ni and 33.8% Ni and reducing the average in proportion to the reduced amount of iron in our material. This 0.128 $k_{\rm B}$/atom result is comparable to the value of $S_{mag}^{\Delta T} = 0.086\ k_B$/atom reported in [5], again after scaling their reported value for the iron concentration. The change in entropy below the Curie pressure resulting from the decrease in magnetization as determined from Eq. (6) is shown in Fig. 5, for both values of $S_{\rm mag}^{\Delta T}$.

It is known from [5, 51, 52] that the magnetic structure in Fe rich fcc Fe-Ni alloys is dominated by the Fe atoms, with only a minor contribution from Ni. From [52, 53] we know that pressure has a minor influence on the alignment of the Ni magnetic moments, and contributes minimally to the magnetic entropy. Therefore, the change in magnetic entropy under pressure $\Delta \mathrm{S_{mag}}(P)$ of Fig. 5 from NFS accounts for nearly all the change in magnetism in $Fe_{55}Ni_{45}$.

IV. DISCUSSION

Figure 5 shows the phonon entropy $S_{\rm ph}(P)$, the change in magnetic entropy $\Delta S_{\rm mag}(P)$, and their sum, $S_{\rm sum}(P)$. Between the pressures of 7 and 13 GPa, $S_{\rm sum}(P)$ is a nearly constant. This pressure range is the region of low thermal expansion observed by synchrotron XRD under pressure (Fig. 1 inset). The separate contributions to thermal expansion (β) from phonons, spins, and their sum are shown in Fig. 6. Below 7 GPa, $\beta_{\rm ph}(P)$ is approximately $+3 \times 10^{-5} K^{-1}$ and $\beta_{\rm mag}(P)$ is negligible. This is again the case for pressures greater than 13 GPa. From 7 to 13 GPa, the magnitude of $\beta_{\rm ph}(P)$ remains approximately constant, but $\beta_{\rm mag}(P)$ increases to

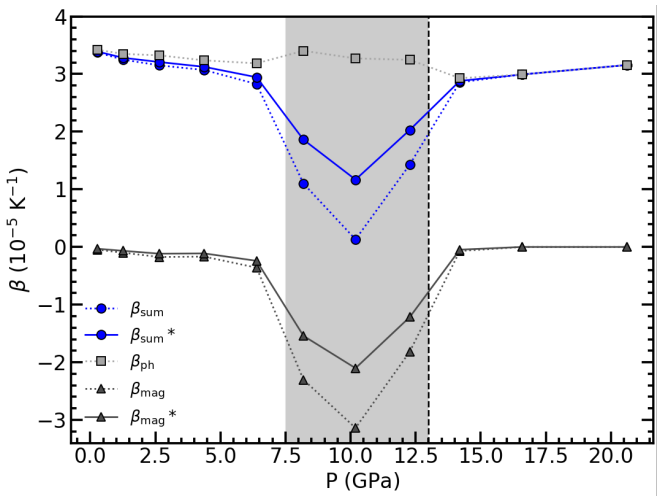

FIG. 6. Pressure dependence of the coefficient of thermal expansion (CTE) from the individual contributions of phonons (squares), magnetism (triangles), and their sum (circles) to Eq. (4). The shaded area represents the range of the pressure induced Invar effect. The dashed vertical line marks the Curie pressure. The $\beta_{\rm mag}$ and $\beta_{\rm sum}$ were determined with $S_{\rm mag}^{\Delta T}$ from [41]. The $\beta_{\rm mag}{}^{*}$ and $\beta_{\rm sum}{}^{*}$ were determined with $S_{\rm mag}^{\Delta T}$ from [5].

$-3{\times}10^{-5} K^{-1}$. This cancellation of $\beta_{\rm ph}(P)$ from phonons and $\beta_{\rm mag}(P)$ from magnetism accounts for the low thermal expansion in the range of the pressure-induced Invar effect. The magnetic entropy changes most rapidly with pressure just below the Curie pressure, contributing to the thermal expansion by Eq. (4). At pressures above the Curie transition, and well below, phonons are the main source of thermal expansion.

Figure 7 shows the coefficient of thermal expansion (CTE) from synchrotron XRD measurements under pressure, compared to the CTE derived from the contributions of phonons and magnetism from Eq. (4). The agreement between the two independent methods for determining the pressure dependence of thermal expansion is good, with the largest discrepancy being caused by uncertainty in the magnetic entropy of the Curie transition.

The phonon entropy of Fig. 5, $S_{\rm ph}$, is nearly monotonic with pressure. Figure 2 shows there is an overall stiffening of the phonon DOS at all pressures. Through the Curie transition, the lower-energy transverse modes continue to stiffen with pressure, although these changes are small. Changes in the phonon DOS near the Curie pressure, when the magnetization is changing rapidly, are an indication of a spin-phonon interaction. Specifically, in the pressure range of 7.2 to 12.8 GPa, the position of the peak from the longitudinal modes remains nearly constant and does not increase with pressure. This peak is marked with the vertical dashed line in Fig. 2, and Fig. S4 in the Supplemental Material [42] shows this by comparing pairs of phonon DOS spectra with differences of 2 GPa in pressure. A similar behavior of the longitu-

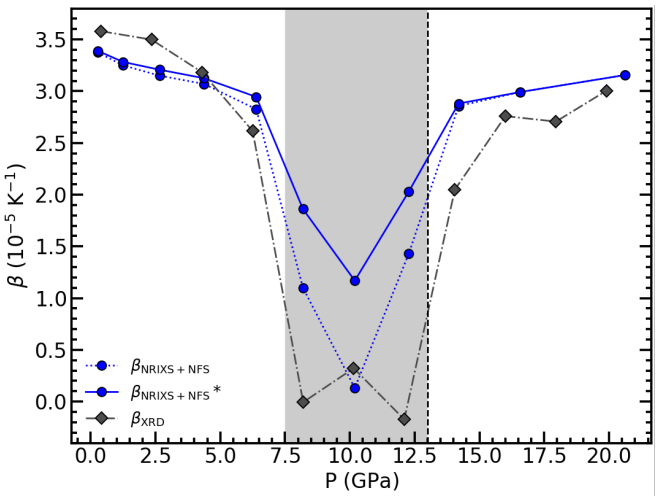

FIG. 7. Pressure dependence of the coefficient of thermal expansion (CTE) from the individual contributions of phonons and magnetism (circles) compared to the measured CTE by synchrotron XRD (diamonds) Shading marks the region of the pressure-induced Invar effect. $\beta_{\mathrm{NRIXS+NFS}}$ was determined with $S_{\mathrm{mag}}^{\Delta T}$ values from [41] and $\beta_{\mathrm{NRIXS+NFS}}{}^{*}$ was determined with $S_{\mathrm{mag}}^{\Delta T}$ values from [5].

dinal peak was found in $Fe_{65}Ni_{35}$ Invar below the Curie pressure, and computational research showed that a spin-phonon interaction was needed to account for it [5]. A definitive proof of a spin-phonon interaction in $Fe_{55}Ni_{45}$ cannot be made solely with the present experimental results, however. Ab initio calculations of spin-phonon interactions in alloys are challenging [5, 54, 55] but they are emerging.

A comparison between the present data on $Fe_{55}Ni_{45}$ and the prior results on $Fe_{65}Ni_{35}$ Invar [5] highlights interesting features of Invar behavior in Fe-Ni. The pressure-induced Invar behavior in $Fe_{55}Ni_{45}$ has a lower bound in pressure, unlike the case for $Fe_{65}Ni_{35}$ Invar, which begins at ambient pressure. Perhaps the key difference between the two materials is that the Curie pressure, P_{C}, of 13 GPa in $Fe_{55}Ni_{45}$ is higher than the P_{C} of 4.6 GPa in $Fe_{65}Ni_{35}$ by nearly a factor of 3. With total magnetic entropies that are similar, the change of magnetic entropy with pressure is spread over a range in pressure that is approximately three times wider, so the magnetic contribution to thermal expansion should be smaller in $Fe_{55}Ni_{45}$ than in $Fe_{65}Ni_{35}$.

With pressure, the more gradually changing $\partial S_{\mathrm{mag}}/\partial P$ for $Fe_{55}Ni_{45}$ is expected to be competitive with the $\partial S_{\mathrm{vib}}/\partial P$ at pressures approaching P_{C} where $M(P)$ changes more rapidly. Indeed, the region of anomalous thermal expansion in $Fe_{55}Ni_{45}$ extends from 7.5 GPa to nearly the P_{C} of 13 GPa, a range of 5.5 GPa. In contrast, the region of Invar behavior in $Fe_{65}Ni_{35}$ is approximately 0 to 3 GPa, about half this range. The Invar behavior in $Fe_{65}Ni_{35}$ does not extend to P_{C} because its $\partial S_{\mathrm{mag}}/\partial P$ and $\partial S_{\mathrm{vib}}/\partial P$ both become large between 3 and 4.6 GPa. Although they retain their opposite signs, the cancellation of their large magnitudes is not sufficiently precise. The magnetization decreases rapidly in a small pressure range near P_{C} in $Fe_{65}Ni_{35}$ Invar. Curiously, there is also a significant change in $\partial S_{\mathrm{vib}}/\partial P$ from spin-phonon interactions in this same range of magnetic disordering. The evidence for spin-phonon coupling in $Fe_{55}Ni_{45}$ is less distinct because the spins become disordered over a broader range of pressure, and the change in spin-phonon coupling is, therefore, more gradual. It is not clear if the spin-phonon interaction in $Fe_{55}Ni_{45}$ differs significantly from that in $Fe_{65}Ni_{35}$, but its change with pressure is less obvious.

V. CONCLUSION

A pressure-induced Invar effect in $Fe_{55}Ni_{45}$ was confirmed by synchrotron XRD measurements at RT and 392 K, where a low thermal expansion was observed from 7 to 13 GPa. The contributions of phonons and magnetism to the thermal expansion of $Fe_{55}Ni_{45}$ were determined by obtaining entropies of phonons and spins from NRIXS and NFS measurements. From 7 GPa to 13 GPa, a rapid change in magnetic entropy from the disordering of spins was observed, giving a thermal expansion that opposed the more monotonic contribution of thermal expansion from phonons. The pressure-induced Invar effect in $Fe_{55}Ni_{45}$ is a consequence of this cancellation of the thermodynamic contributions to thermal expansion from phonons and spins. The phonon DOS of $Fe_{55}Ni_{45}$ showed an arrest of the stiffening with pressure of the longitudinal phonon modes, indicative of a spin-phonon coupling.

ACKNOWLEDGMENTS

This work was supported by the National Science Foundation under grant no. 1904714 (P.G., S.H.L., C.M.B-C., and B.F.). P.G. acknowledges support of the NSF Graduate Research Fellowship DGE-1745301. This research used resources of the APS, a US DOE Office of Science User Facility operated for the DOE Office of Science by Argonne National Laboratory under Contract No. DE-AC02-06CH11357 (P.G., S.H.L., C.M.B-C., and B.F.). HPCAT operations are supported by DOE-NNSA's Office of Experimental Sciences. Use of the COMPRES-GSECARS gas-loading system was supported by COMPRES under NSF Cooperative Agreement EAR 1606856 and by GSECARS through NSF Grant No. EAR-1634415 and DOE Grant No. DE-FG02-94ER14466. We thank C. Li for assistance with the pressure cells and E. Priesen Reis for assistance with magnetization measurements.

REFERENCES

[1] C.-É. Guillaume, *Recherches sur les aciers au nickel.* Dilatations aux temperatures elevees; resistance electrique. C. R. Acad. Sci. **125**, 235–238 (1897).

[2] C.-É. Guillaume, The anomaly of the nickel-steels, Proceedings of the Physical Society of London, **32**, 374, (1919).

[3] C.-É. Guillaume, Nobel Lecture in Physics, `https://www.nobelprize.org/uploads/2018/06/guillaume-lecture.pdf`, (1920).

[4] E. Wasserman, Invar: Moment-volume instabilities in transition metals and alloys, Handbook of Ferromagnetic Materials, **5**, 237–322, (1990).

[5] S. H. Lohaus, M. Heine, P. Guzman, C. M. Bernal-Choban, C. N. Saunders, G. Shen, O. Hellman, D. Broido, and B. Fultz, A thermodynamic explanation of the Invar effect, Nature Physics, **19**, 1642–1648, (2023).

[6] K. Sumiyama, M. Shiga, M. Morioka, and Y. Nakamura, Characteristic magnetovolume effects in Invar type Fe-Pt alloys, Journal of Physics F: Metal Physics, **9**, 1665, (1979).

[7] Y. Nakamura, K. Sumiyama, and M. Shiga, Fe-Pt Invar alloys—homogeneous strong ferromagnets, Journal of Magnetism and Magnetic Materials, **12**, 127–134, (1979).

[8] M. Takahashi, F. Ono, and K. Takakura, The Invar characteristics on Co-Fe alloys, AIP Conference Proceedings, **29**, 562–563, (1976).

[9] B. Gehrmann, M. Acet, H. Herper, E. Wassermann, and W. Pepperhoff, The Invar Property of Elemental FCC Co and Large Spontaneous Magnetostriction of BCC Fe-Co, Physica Status Solidi (B), **214**, 175–185, (1999).

[10] G. Hausch, Invar-like thermal expansion anomaly in antiferromagnetic Mn-Ni alloys, Physica Status Solidi (A), **41**, K35–K38, (1977).

[11] T. Yokoyama and K. Eguchi, Anisotropic thermal expansion and cooperative Invar and anti-Invar effects in Mn alloys, Physical Review Letters, **110**, 075901, (2013).

[12] Y. V. Ergin, Anomalies in the Temperature Dependence of the Thermal Expansion Coefficient of a Gadolinium Single Crystal, Soviet Physics JETP, **21**, 709–710, (1965).

[13] R. M. Bozorth and T. Wakiyama, Magnetostriction and anomalous thermal expansion of single crystals of gadolinium, Journal of the Physical Society of Japan, **18**, 97–106, (1963).

[14] F. Barson, S. Legvold, and F. H. Spedding, Thermal expansion of rare earth metals, Physical Review, **105**, 418, (1957).

[15] A. V. Ruban, S. Khmelevskyi, P. Mohn, and B. Johansson, Magnetic state, magnetovolume effects, and atomic order in $Fe_{65}Ni_{35}$ Invar alloy: A first principles study, Physical Review B, **76**, 014420, (2007).

[16] A. Menshikov, On the Invar problem, Physica B: Condensed Matter, **161**, 1–8, (1990).

[17] A. Sahoo and V. Medicherla, Fe-Ni Invar alloys: A review, Materials today: proceedings, **43**, 2242–2244, (2021).

[18] E. Wassermann, The Invar problem, Journal of Magnetism and Magnetic Materials, **100**, 346–362, (1991).

[19] Y. Nakamura, The Invar problem, IEEE Transactions on Magnetics, **100**, 278–291, (1976).

[20] L. Dubrovinsky, N. Dubrovinskaia, I. A. Abrikosov, M. Vennström, F. Westman, S. Carlson, M. van Schilfgaarde, and B. Johansson, Pressure-induced invar effect in Fe-Ni alloys, Physical Review Letters, **86**, 4851, (2001).

[21] M. Winterrose, M. Lucas, A. Yue, I. Halevy, L. Mauger, J. Muñoz, J. Hu, M. Lerche, and B. Fultz, Pressure-induced invar behavior in Pd_3Fe, Physical Review Letters, **102**, 237202, (2009).

[22] M. Winterrose, L. Mauger, I. Halevy, A. Yue, M. Lucas, J. Muñoz, H. Tan, Y. Xiao, P. Chow, W. Sturhahn, *et al.*, Dynamics of iron atoms across the pressure-induced Invar transition in Pd_3Fe, Physical Review B, **83**, 134304, (2011).

[23] J. Leger, C. Loriers-Susse, and B. Vodar, Pressure effect on the curie temperatures of transition metals and alloys, Physical Review B, **6**, 4250, (1972).

[24] G. Hausch, Magnetovolume effects in invar alloys: Pressure dependence of the curie temperature, Physica Status Solidi (A), **16**, 371–376, (1973).

[25] G. Oomi and N. Mori, High Pressure X-Ray Study of Anomalous Bulk Modulus of an $Fe_{70}Ni_{30}$ Invar Alloy, Journal of the Physical Society of Japan, **50**, 1043–1044, (1981).

[26] M. Abd-Elmeguid, B. Schleede, and H. Micklitz, Pressure-induced antiferromagnetism in fcc Fe-Ni Invar alloys, Journal of Magnetism and Magnetic Materials, **72**, 253–257, (1988).

[27] M. Abd-Elmeguid and H. Micklitz, Observation of a pressure-induced collapse of the Fe magnetic moment in the strong itinerant ferromagnet $Fe_{72}Pt_{28}$, Physical Review B, **40**, 7395, (1989).

[28] Y. Abdu, H. Annersten, L. Dubrovinsky, and N. Dubrovinskaia, High Pressure Mössbauer Studies on fcc $Fe_{53}Ni_{47}$ Alloy, Hyperfine Interactions, **156**, 389–394, (2004).

[29] Ll. Mañosa, G. Saunders, H. Rahdi, U. Kawald, J. Pelzl, and H. Bach, Acoustic-mode vibrational anharmonicity related to the anomalous thermal expansion of Invar iron alloys, Physical Review B, **45**, 2224, (1992).

[30] M. Schwoerer-Böhning, S. Klotz, J. Besson, E. Burkel, M. Braden, and L. Pintschovius, The pressure dependence of the TA1 [110] phonon frequencies in the ordered Invar alloy Fe3Pt at pressures up to 7 GPa, Europhysics Letters, **33**, 679, (1996).

[31] S. Odin, F. Baudelet, J. Itié, A. Polian, S. Pizzini, A. Fontaine, C. Giorgetti, E. Dartyge, and J. Kappler, Experimental evidence of pressure-induced magnetic phase transition in $Fe_{72}Pt_{28}$ Invar alloy, Journal of Applied Physics, **83**, 7291–7293, (1998).

[32] S. Odin, F. Baudelet, C. Giorgetti, E. Dartyge, J. Itié, A. Polian, J. Chervin, S. Pizzini, A. Fontaine, and J. Kappler, Magnetic phase transitions in $Fe_{72}Pt_{28}$ Invar compound studied by high-pressure X-ray magnetic circular

dichroism and X-ray diffraction, Europhysics Letters, **47**, 378, (1999).

[33] J.-P. Rueff, A. Shukla, A. Kaprolat, M. Krisch, M. Lorenzen, F. Sette, and R. Verbeni, Magnetism of Invar alloys under pressure examined by inelastic X-ray scattering, Physical Review B, **63**, 132409, (2001).

[34] M. Matsushita, T. Nishimura, S. Endo, M. Ishizuka, K. Kindo, and F. Ono, Anomalous magnetic moments in Fe–Pt and Fe–Pd Invar alloys under high pressure, Journal of Physics: Condensed Matter, **14**, 10753, (2002).

[35] M. Matsushita, S. Endo, K. Miura, and F. Ono, Pressure-induced change of the magnetic state in ordered Fe–Pt Invar alloy, Journal of Magnetism and Magnetic Materials, **269**, 393–397, (2004).

[36] M. Matsushita, Y. Nakamoto, E. Suzuki, Y. Miyoshi, H. Inoue, S. Endo, T. Kikegawa, and F. Ono, The lattice softening and the crystal structure of Fe–Pt Invar alloys under high pressures, Journal of Magnetism and Magnetic Materials, **284**, 403–408, (2004).

[37] M. Matsushita, Y. Miyoshi, S. Endo, and F. Ono, Pressure-induced magnetic phase transitions in Fe-based Invar alloys, Physical Review B, **72**, 214404, (2005).

[38] F. Decremps and L. Nataf, Abrupt discontinuity of the bulk modulus pressure dependence in $Fe_{64}Ni_{36}$, Physical Review Letters, **92**, 157204, (2004).

[39] L. Nataf, F. Decremps, M. Gauthier, and B. Canny, High-pressure structural study of $Fe_{64}Ni_{36}$ and $Fe_{72}Pt_{28}$ Invar alloys at low-temperature, Physical Review B, **74**, 184422, (2006).

[40] P. Gorria, D. Martínez-Blanco, M. J. Pérez, J. A. Blanco, A. Hernando, M. A. Laguna-Marco, D. Haskel, N. Souza-Neto, R. I. Smith, W. G. Marshall, *et al.*, Stress-induced large Curie temperature enhancement in $Fe_{64}Ni_{36}$ Invar alloy, Physical Review B, **80**, 064421, (2009).

[41] Y. Tanji, H. Asano, and H. Moriya, Specific Heats of Fe-Ni(fcc) Alloys at High Temperatures, Science Rep. Research Inst. Tohoku Univ., **24**, 205–217, (1973).

[42] See Supplemental Material at [URL will be inserted by publisher] for details on the measurements and thermodynamics of the "Elinvar" effect in $Fe_{55}Ni_{45}$, effects of pressure on the phonon DOS, temperature dependence of the normalized magnetization, and hyperfine magnetic field distributions. The Supplemental Material also contains Refs. [1–5, 41].

[43] M. Rivers, V. B. Prakapenka, A. Kubo, C. Pullins, C. M. Holl, and S. D. Jacobsen, The COMPRES/GSECARS gas-loading system for diamond anvil cells at the Advanced Photon Source, High Pressure Research, **28**, 273–292, (2008).

[44] R. Hrubiak, S. Sinogeikin, E. Rod, and G. Shen, The laser micro-machining system for diamond anvil cell experiments and general precision machining applications at the High Pressure Collaborative Access Team, Review of Scientific Instruments, **86**, 072202, (2015).

[45] W. Sturhahn, Nuclear resonant spectroscopy, Journal of Physics: Condensed Matter, **16**, S497, (2004).

[46] W. Sturhahn, CONUSS and PHOENIX: Evaluation of nuclear resonant scattering data, Hyperfine Interactions, **125**, 149–172, (2000).

[47] M. Lucas, L. Mauger, J. Muñoz, I. Halevy, J. Horwath, S. Semiatin, S. Leontsev, M. B. Stone, D. L. Abernathy, Y. Xiao, *et al.*, Phonon densities of states of face-centered-cubic Ni-Fe alloys, Journal of Applied Physics, **113**, 17A308, (2013).

[48] B. Fultz, *Phase transitions in materials* (Cambridge University Press, 2020).

[49] M. Kobeissi, Mössbauer study of static and dynamic critical behavior in Fe, Physical Review B, **24**, 2380, (1981).

[50] S. H. Lohaus, M. B. Johnson, P. F. Ahnn, C. N. Saunders, H. L. Smith, M. A. White, and B. Fultz, Thermodynamic stability and contributions to the Gibbs free energy of nanocrystalline Ni_3Fe, Physical Review Materials, **4**, 086002, (2020).

[51] I. A. Abrikosov, A. E. Kissavos, F. Liot, B. Alling, S. Simak, O. Peil, and A. V. Ruban, Competition between magnetic structures in the Fe rich fcc FeNi alloys, Physical Review B, **76**, 014434, (2007).

[52] M. van Schilfgaarde, I. A. Abrikosov, and B. Johansson, Origin of the Invar effect in iron–nickel alloys, Nature, **400**, 46–49, (1999).

[53] K. Matsumoto, H. Maruyama, N. Ishimatsu, N. Kawamura, M. Mizumaki, T. Irifune, and H. Sumiya, Non-collinear spin structure in Fe–Ni invar alloy probed by magnetic EXAFS at high pressure, Journal of the Physical Society of Japan, **80**, 023709, (2011).

[54] M. Heine, O. Hellman, D. Broido, Theory of thermal properties of magnetic materials with unknown entropy, Physical Review Materials, **6**, 113805, (2022).

[55] A. Ehn, B. Alling, I.A. Abrikosov, First-principles theory of the pressure-induced invar effect in FeNi alloys, Physical Review B, **107**, 104422, (2023).